

Towards Visually Explaining Similarity Models

Meng Zheng^{1,2}, Srikrishna Karanam¹, Terrence Chen¹, Richard J. Radke², and Ziyuan Wu¹

¹ United Imaging Intelligence, Cambridge MA, USA

² Rensselaer Polytechnic Institute, Troy NY, USA

{first.last}@united-imaging.com, rjradke@ecse.rpi.edu

Abstract. We consider the problem of visually explaining similarity models, *i.e.*, explaining why a model predicts two images to be similar in addition to producing a scalar score. While much recent work in visual model interpretability has focused on gradient-based attention, these methods rely on a classification module to generate visual explanations. Consequently, they cannot readily explain other kinds of models that do not use or need classification-like loss functions (*e.g.*, similarity models trained with a metric learning loss). In this work, we bridge this crucial gap, presenting the first method to generate gradient-based visual explanations for image similarity predictors. By relying solely on the learned feature embedding, we show that our approach can be applied to any kind of CNN-based similarity architecture, an important step towards generic visual explainability. We show that our resulting visual explanations serve more than just interpretability; they can be infused into the model learning process itself with new trainable constraints based on our similarity explanations. We show that the resulting similarity models perform, and can be visually explained, better than the corresponding baseline models trained without our explanation constraints. We demonstrate our approach using extensive experiments on three different kinds of tasks: generic image retrieval, person re-identification, and low-shot semantic segmentation.

1 Motivation and Contributions

As we work towards transitioning algorithmic deep learning research to real-world applications, we must consider the important question of model explainability and interpretability. This is especially critical for applications such as healthcare where medical professionals may not readily trust the decisions of a black box artificial intelligence system for diagnostic purposes.

Following the visualization work of Zeiler and Fergus [1] and Mahendran and Vedaldi [2], much recent progress in visually explaining convolutional neural networks (CNNs) has been led by attention-based techniques [3,4] that produce attention maps highlighting regions in input images that are considered (by the

* This work was done during M. Zheng’s internship with United Imaging Intelligence, Cambridge MA, USA. Corresponding author: Srikrishna Karanam.

model) to be important for the final prediction. GradCAM [4] has been particularly impactful with its simple and intuitive attention generation mechanism as well as extensibility in using the resulting attention to enforce trainable constraints [5,6]. While “attention” may have different connotations [7,8,9,10], in our work, we refer to attention computed by means of the gradient of a differentiable activation in the spirit of GradCAM. A key limitation of GradCAM, and other related methods, is that they rely on activations from a classification module (*e.g.*, a fully-connected unit followed by softmax) to generate the attention map. While there are many models in computer vision that rely on a classification loss function during training, there are even more that do not need one (*e.g.*, generative models, autoencoders, similarity models). While it is desirable to explain a wide variety of models (not just classification ones), extending gradient-based explanation methods to these models is not trivial. Furthermore, adding a classification loss function just for the sake of computing attention maps to (for example) a similarity model that is typically trained with a metric learning loss seems suboptimal. Consequently, the question we ask is: *can we generate visual explanations for models without needing a classification module for computing visual attention?* Here, we address this question in the context of similarity models trained on image data.

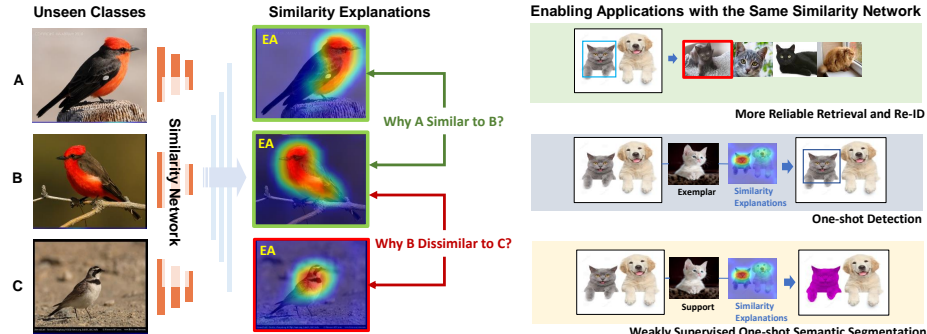


Fig. 1. We propose to visually explain similarity models, showing our method’s versatility in diverse applications such as metric learning and semantic segmentation.

A similarity model is trained to embed same-category images close together in the learned feature space while embedding images from different categories farther apart. This is typically achieved using a metric learning loss. Our definition of a visual explanation for such a model is a set of attention maps that highlights regions in the input images that represent the model’s evidence that the images are similar, *i.e.*, close in the learned feature space. For instance, in the case of a Siamese similarity model (trained with pairs of data), we will generate two attention maps highlighting regions that the model reasons are most important for a particular pair to be similar. Similarly, for a triplet similarity

model (trained with triplets of data), we will generate three attention maps that highlight regions that the model reasons are most important for this particular input to satisfy the triplet condition (i.e., the anchor image is close to the positive image but far from the negative image). We refer to such sets of attention maps as **similarity attention** (see Fig. 1). As noted above, one can certainly add a classification module to a similarity model so that the resulting classification activations can be used to generate attention maps with GradCAM. In Fig. 2, we show the result of this operation (this Siamese model was trained with the contrastive and binary cross entropy loss), where we see the GradCAM attention maps highlighting non-corresponding (red) regions for the similar pair whereas our proposed similarity attention more clearly highlights corresponding regions. Comparing these two figures, it is clear that simply adding a classification term so one can use GradCAM to generate attention does not result in the kind of intuitively satisfying explanations one would expect; our proposed method explicitly bridges this gap.

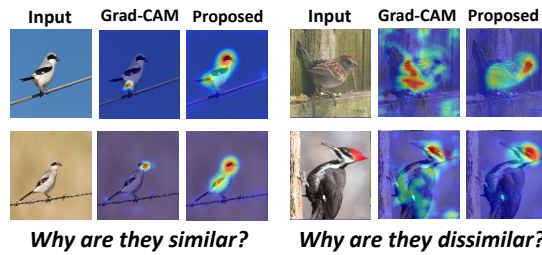


Fig. 2. GradCAM vs. Proposed.

identifying feature dimensions that are important for two similar images to be embedded close in the feature space. Starting from such analysis, we propose to generate a differentiable activation that can be used to compute gradients with respect to convolutional feature maps and hence attention maps, or similarity attention as noted above. A useful by-product of this approach, leading to our next contribution, is that these visual explanations result in explicit constraints, called **similarity mining**, for further bootstrapping the learning of the similarity model, which we demonstrate results in improved downstream performance (*e.g.*, better rank performance) as well as attention maps.

In order to demonstrate technical generality, we show how our method can be used to generate attention maps for a variety of similarity architectures (*e.g.*, Siamese, triplet, quadruplet). We do this both theoretically, deriving raw attention matrices conditioned on the learned feature space, and empirically. In order to demonstrate wide applicability, we conduct experiments on three different tasks: generic image retrieval, person re-identification (re-id), and low-shot semantic segmentation. While retrieval and re-id are standard metric learning

Our method does not need a classification module to generate attention maps, thereby addressing a key limitation of GradCAM. Furthermore, as shown in Fig 2, our method produces more intuitive visual explanations for similarity models, thereby removing the need for training the similarity model with a classification objective just to compute attention maps. Instead, our approach is based on identi-

applications, the segmentation application shows how our proposed visual explanations can do more than just explain why two images are similar. Specifically, we demonstrate how they can be used as cues to discover corresponding regions of interest (in this case between a query and a support image) and perform semantic segmentation, as overviewed in Fig. 1.

2 Method

Given N labeled images $\{(\mathbf{x}_i, y_i)\}$ each belonging to one of k categories, where $i = 1, \dots, N$, $\mathbf{x} \in \mathbb{R}^{H \times W \times c}$, and $y \in \{1, \dots, k\}$, we propose a method to visually explain why a similarity model predicts two images \mathbf{x}_1 and \mathbf{x}_2 to be similar. In Section 2.1, we discuss our proposed technique to generate these visual similarity explanations and show how it can be easily integrated with existing similarity models. In Section 2.2, we discuss how our proposed explanation generation mechanism facilitates principled training of similarity models with our new similarity mining learning objective.

2.1 Generating visual similarity explanations

Traditional similarity predictors such as Siamese or triplet models are trained to respect the relative ordinality of distances between data points. For instance, given a training set of triplets $\{(\mathbf{x}_i^a, \mathbf{x}_i^p, \mathbf{x}_i^n)\}$, where $(\mathbf{x}_i^a, \mathbf{x}_i^p)$ have the same categorical label while $(\mathbf{x}_i^a, \mathbf{x}_i^n)$ belong to different classes, a triplet similarity predictor learns a d -dimensional feature embedding of the input \mathbf{x} , $f(\mathbf{x}) \in \mathbb{R}^d$, such that the distance between $f(\mathbf{x}_i^a)$ and $f(\mathbf{x}_i^n)$ is larger than that between $f(\mathbf{x}_i^a)$ and $f(\mathbf{x}_i^p)$ (within a predefined margin α). Starting from such a baseline predictor (*e.g.*, triplet), our key insight is that we can use the model’s learned feature embedding to generate visual explanations, in the form of attention maps, for why the current input triplet satisfies the triplet criterion. We refer to this set of attention maps as *similarity attention*. Note that our idea of generating attention maps conditioned on the feature embedding is different from existing work [4,11] that rely on an extra classification module (and the classification logits) to obtain the attention maps. In our case, we are not limited by this requirement, instead computing a score directly from the feature vectors to generate the explanations. A crucial advantage with this proposed strategy is the resulting flexibility and generality in visually explaining any feature embedding network, as discussed in the next section.

Given a triplet $(\mathbf{x}^a, \mathbf{x}^p, \mathbf{x}^n)$, we first extract feature vectors $f(\mathbf{x}^a)$, $f(\mathbf{x}^p)$, and $f(\mathbf{x}^n)$ (denoted \mathbf{f}^a , \mathbf{f}^p , and \mathbf{f}^n respectively going forward, all normalized to have unit l_2 norm). A perfectly trained triplet similarity model must result in \mathbf{f}^a , \mathbf{f}^p , and \mathbf{f}^n satisfying the triplet criterion. Under this scenario, local differences in the image space will roughly correspond to proportional differences in the feature space, and hence there must exist some feature dimensions contributing the most to the triplet criterion being respected. Our idea is to generate the visual explanations conditioned on these feature dimensions. To this end, we

compute the absolute differences and construct the weight vectors \mathbf{w}^p and \mathbf{w}^n as $\mathbf{w}^p = \mathbf{1} - |\mathbf{f}^a - \mathbf{f}^p|$ and $\mathbf{w}^n = |\mathbf{f}^a - \mathbf{f}^n|$. With \mathbf{w}^p , we seek to highlight the feature dimensions that have a small absolute difference value (*e.g.*, for those dimensions t , \mathbf{w}_t^p will be closer to 1), whereas with \mathbf{w}^n we seek to highlight the feature dimensions with large absolute differences. Given \mathbf{w}^p and \mathbf{w}^n , we construct a single weight vector $\mathbf{w} = \mathbf{w}^p \odot \mathbf{w}^n$, where \odot denotes the element-wise product operation. With \mathbf{w} , we obtain a higher weight with feature dimensions that have a high value in both \mathbf{w}^p and \mathbf{w}^n . In other words, we focus on elements that contribute the most to the positive feature pair being close and the negative feature pair being further away (*i.e.*, contributing to the triplet criterion) and then determine attention maps. Specifically, we first calculate the dot product of \mathbf{w} with each of \mathbf{f}^a , \mathbf{f}^p , and \mathbf{f}^n to get the sample scores $s^a = \mathbf{w}^T \mathbf{f}^a$, $s^p = \mathbf{w}^T \mathbf{f}^p$, and $s^n = \mathbf{w}^T \mathbf{f}^n$ for each image in the triplet $(\mathbf{x}^a, \mathbf{x}^p, \mathbf{x}^n)$. We then calculate the gradients of these scores with respect to the image's convolutional feature maps to get its attention map. Specifically, given a score s^i , $i \in \{a, p, n\}$, the attention map $\mathbf{M}^i \in \mathbb{R}^{m \times n}$ is determined as:

$$\mathbf{M}^i = \text{ReLU} \left(\sum_k \alpha_k \mathbf{A}_k \right) \quad (1)$$

where $\mathbf{A}_k \in \mathbb{R}^{m \times n}$ is the k^{th} ($k = 1, \dots, c$) convolutional feature channel (from an intermediate layer) of the feature map $\mathbf{A} \in \mathbb{R}^{m \times n \times c}$ and $\alpha_k = \text{GAP} \left(\frac{\partial s^i}{\partial \mathbf{A}_k} \right)$, while GAP refers to global average pooling.

Extensions to other architectures Our method is not limited to triplet CNNs and is extensible to other kinds of similarity architectures. For a Siamese model, the inputs are pairs $(\mathbf{x}^1, \mathbf{x}^2)$. Given their feature vectors \mathbf{f}^1 and \mathbf{f}^2 , we compute the weight vector \mathbf{w} in the same way as the triplet scenario. If \mathbf{x}^1 and \mathbf{x}^2 belong to the same class, $\mathbf{w} = \mathbf{1} - |\mathbf{f}^1 - \mathbf{f}^2|$, otherwise, $\mathbf{w} = |\mathbf{f}^1 - \mathbf{f}^2|$. With \mathbf{w} , and the sample scores $s^1 = \mathbf{w}^T \mathbf{f}^1$ and $s^2 = \mathbf{w}^T \mathbf{f}^2$, we compute attention maps \mathbf{M}^1 and \mathbf{M}^2 for \mathbf{x}^1 and \mathbf{x}^2 respectively using Equation 1.

For a quadruplet model, the inputs are quadruplets $(\mathbf{x}^a, \mathbf{x}^p, \mathbf{x}^{n1}, \mathbf{x}^{n2})$, where \mathbf{x}^p is the positive sample and \mathbf{x}^{n1} and \mathbf{x}^{n2} are negative samples with respect to the anchor \mathbf{x}^a . Here, we compute the three difference feature vectors $\mathbf{f}^1 = |\mathbf{f}^a - \mathbf{f}^p|$, $\mathbf{f}^2 = |\mathbf{f}^a - \mathbf{f}^{n1}|$, and $\mathbf{f}^3 = |\mathbf{f}^a - \mathbf{f}^{n2}|$. Following the intuition described in the triplet case, we compute the difference weight vectors as $\mathbf{w}^1 = \mathbf{1} - \mathbf{f}^1$ for the positive pair and $\mathbf{w}^2 = \mathbf{f}^2$ and $\mathbf{w}^3 = \mathbf{f}^3$ for the two negative pairs. The overall weight vector \mathbf{w} is then computed as the element-wise product of the three individual weight vectors: $\mathbf{w} = \mathbf{w}^1 \odot \mathbf{w}^2 \odot \mathbf{w}^3$. With \mathbf{w} , and the sample scores $s^a = \mathbf{w}^T \mathbf{f}^a$, $s^p = \mathbf{w}^T \mathbf{f}^p$, $s^{n1} = \mathbf{w}^T \mathbf{f}^{n1}$, and $s^{n2} = \mathbf{w}^T \mathbf{f}^{n2}$, we use Equation 1 to obtain the four attention maps \mathbf{M}^a , \mathbf{M}^p , \mathbf{M}^{n1} , and \mathbf{M}^{n2} .

For other models trained with custom metric learning losses, all one has to do is compute feature vectors. The weight vector and sample scores, and hence attention maps, can then be easily determined as above. Given this dependence on

just the feature embedding (obtainable universally for any CNN-based similarity architecture), our method is applicable to generic similarity models.

2.2 Learning with similarity mining

With our proposed method, we can generate attention maps to explain the reasoning for a similarity model’s predictions. However, we note all operations leading up to the attention map \mathbf{M}^i in Section 2.1 are differentiable and thus we can use the generated attention maps to further bootstrap the training process. To this end, we propose a new learning objective called *similarity mining*. The goal of similarity mining is to facilitate the complete discovery of local image regions that the model deems necessary to satisfy the similarity criterion.

Given the three attention maps $\mathbf{M}^i, i \in \{a, p, n\}$ (in the triplet case), we up-sample them to be the same size as the input image and perform soft-masking, producing masked images that exclude pixels corresponding to high-response regions in the attention maps. This is realized as: $\hat{\mathbf{x}} = \mathbf{x} \odot (\mathbf{1} - \Sigma(\mathbf{M}))$, where $\Sigma(\mathbf{Z}) = \text{sigmoid}(\alpha(\mathbf{Z} - \beta))$ (all element-wise operations and α and β are constants pre-set by cross validation). These masked images are then fed back to the same encoder of the triplet model to obtain the feature vectors \mathbf{f}^{a*} , \mathbf{f}^{p*} , and \mathbf{f}^{n*} . Our proposed similarity mining loss L_{sm} can then be expressed as:

$$L_{sm} = \left| \|\mathbf{f}^{a*} - \mathbf{f}^{p*}\| - \|\mathbf{f}^{a*} - \mathbf{f}^{n*}\| \right| \quad (2)$$

where $\|\mathbf{t}\|$ represents the Euclidean norm of the vector \mathbf{t} . The intuition here is that by minimizing L_{sm} , the model has difficulties in predicting whether the input triplet would satisfy the triplet condition. This is because as L_{sm} gets smaller, the model will have exhaustively discovered all possible local regions in the triplet, and erasing these regions (via soft-masking above) will leave no relevant features available for the model to predict that the triplet satisfies the criterion.

Extensions to other architectures Like similarity attention, similarity mining is also extensible to other similarity learning architectures. For a Siamese model, given the two attention maps \mathbf{M}^1 and \mathbf{M}^2 , we perform the soft-masking operation described above to obtain the masked images and their feature vectors \mathbf{f}^{1*} and \mathbf{f}^{2*} . The similarity mining objective in this case attempts to maximize the distance between \mathbf{f}^{1*} and \mathbf{f}^{2*} , *i.e.*, $L_{sm} = -|\mathbf{f}^{1*} - \mathbf{f}^{2*}|$. The intuition here is that we seek to get the model to a state where after erasing, the model can no longer predict that the data pair belongs to the same class. This is because as L_{sm} gets smaller, the model will have exhaustively discovered all corresponding regions that are responsible for the data pair to be predicted as belonging to the same class (*i.e.*, low feature space distance), and erasing these regions (via soft-masking) will result in a larger feature space distance between the positive samples.

For a quadruplet model, using the four attention maps, we compute the feature vectors \mathbf{f}^{a*} , \mathbf{f}^{p*} , \mathbf{f}^{n1*} , and \mathbf{f}^{n2*} using the same masking strategy above.

We then consider the two triplets $T_1 = (\mathbf{f}^{a*}, \mathbf{f}^{p*}, \mathbf{f}^{n1*})$ and $T_2 = (\mathbf{f}^{a*}, \mathbf{f}^{p*}, \mathbf{f}^{n2*})$ in constructing the similarity mining objective as $L_{sm} = L_{sm}^{T_1} + L_{sm}^{T_2}$, where $L_{sm}^{T_1}$ and $L_{sm}^{T_2}$ correspond to Equation 2 evaluated for T_1 and T_2 respectively.

2.3 Overall training objective

We train similarity models with both the traditional similarity/metric learning objective L_{ml} (e.g., contrastive, triplet, etc.) as well as our proposed similarity mining objective L_{sm} . Our overall training objective is:

$$L = L_{ml} + \gamma L_{sm} \quad (3)$$

where γ is a weight factor controlling the relative importance of L_{ml} and L_{sm} .

3 Experiments and Results

We conduct experiments on three different tasks: image retrieval (Sec. 3.1), person re-identification (Sec. 3.2), and one-shot semantic segmentation (Sec. 3.3). We use a pretrained ResNet50 as our base architecture and implement all our code in Pytorch. All implementation details are available in the supplemental material.

3.1 Image retrieval

We conduct experiments on the CUB200 (“CUB”) [12], Cars-196 (“CARS”) [13] and Stanford Online Products (“SOP”) [14] datasets. We first discuss qualitative results, *i.e.*, similarity attention maps, obtained with our method. In Figure 3(a), we compare our similarity attention with those of GradCAM for a Siamese model (please note two pairs in each of “baseline” and “mining” sections). As noted in Section 1, the GradCAM attention maps were obtained by training the model with a classification loss (we use binary cross entropy, L_{bce}) in addition to the standard metric learning loss qualitative attention maps (so $L_{ml} + \gamma L_{bce}$ for GradCAM whereas our proposed attention uses only L_{ml}). One can note from Fig. 3(a) (“baseline”) that our similarity attention maps more comprehensively capture the corresponding regions in these images, with high response regions helping explain why the pairs of images are similar. This is not the case with GradCAM, with mostly non-corresponding regions being highlighted. The same observations can be made with models trained with our mining loss as well (“mining” in Fig. 3(a)), but now using L_{bce} to compute attention before calculating the loss in Equation 2 (L_{bce-sm} to highlight GradCAM attention instead of our proposed attention). In other words, here the model is trained with $L_{ml} + \gamma_1 L_{bce} + \gamma_2 L_{bce-sm}$. These results suggest that simply adding a classification loss term to compute attention maps, as in GradCAM, is not enough. Next, to demonstrate generality, in Fig. 3(b), we present our similarity attention maps for various architectures- Siamese, triplet, and quadruplet. In each of these cases,

our method is able to highlight intuitively satisfying regions (*e.g.*, face/neck regions in the triplet case), providing visual evidence for similarity (in the Siamese case) or why they satisfy the training criterion (triplet or quadruplet loss).

To further demonstrate the generalizability in obtaining these visual explanations, in Fig. 4(a), we show our triplet attention maps (for CUB and CARS testing data) with two models- one trained and tested with CUB data and one trained and tested with CARS data. Our proposed method is generally able to highlight intuitively satisfying corresponding regions with both models. For instance, in the right triplet (for birds) of Fig. 4(a) (model trained with CARS), the region around the face is what makes the second bird image similar, and the third bird image dissimilar, to the first (anchor) bird image. These results provide evidence for the generalizability of our generated visual explanations, with even a model not trained on relevant data (trained on CARS but tested on CUB or trained on CUB but tested on CARS) able to discover local regions contributing to the final decision. We also show the impact of our proposed similarity mining loss on the generated attention maps in Fig. 4(b) (left triplet: baseline L_{ml} , right triplet: proposed $L_{ml} + \gamma L_{sm}$). We clearly see that the proposed L_{sm} results in more exhaustive and accurate discovery of local regions, further demonstrating its impact in improving model performance. Additional qualitative results can be found in the supplementary material.

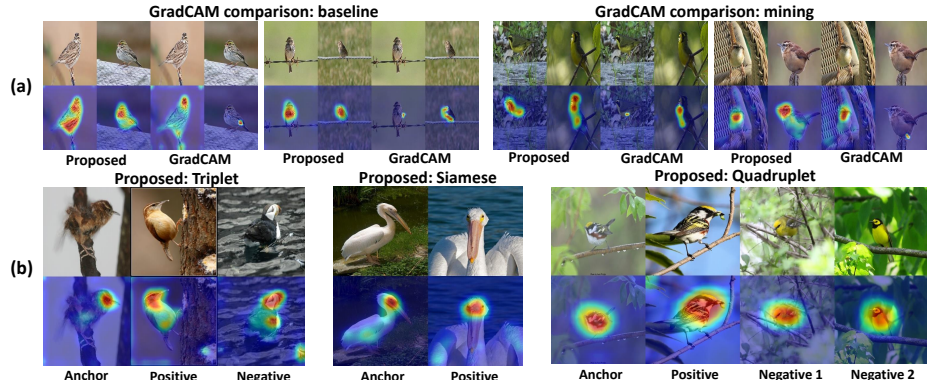


Fig. 3. (a) Proposed similarity attention vs. GradCAM: we show two examples each with baseline and mining. (b) Proposed similarity attention for triplet, Siamese, and quadruplet models.

Finally, we report quantitative performance, following the protocol of Wang *et al.* [20] and using the standard Recall@K (R-K) metric [20]. We show ablation results to demonstrate performance gains achieved by our proposed similarity mining loss of Section 2.2. In Table 1 (Left), we show both baseline (trained only with L_{ml}) and our results with the Siamese, triplet, and quadruplet architectures (trained with $L_{ml} + \gamma L_{sm}$). One can note that our method consistently improves the baseline performance across all three architectures. Finally,

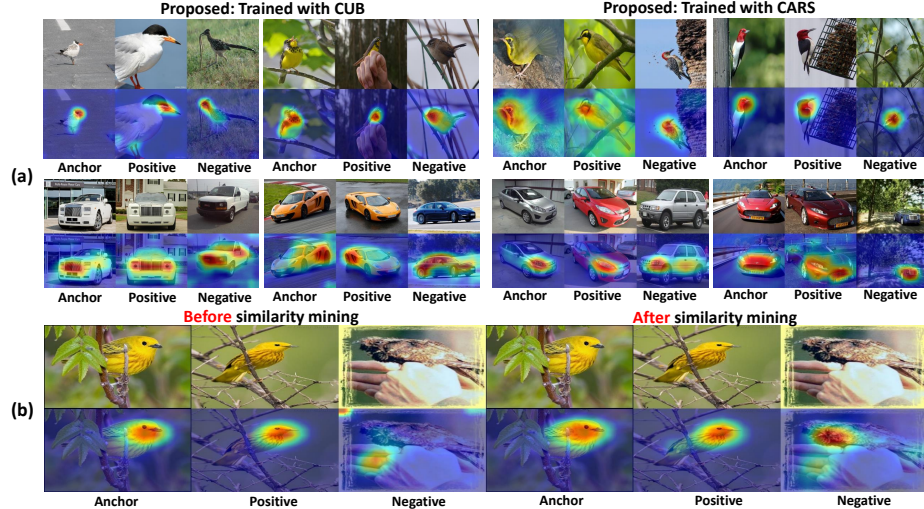


Fig. 4. (a) Triplet attention maps on CUB and CARS with our proposed method for models trained with CUB and CARS. (b) Our triplet attention maps with and without similarity mining.

Arch.	Type	R-1	R-2	R-4
Siamese	Baseline	65.9	77.5	85.8
	Proposed	67.7	77.8	85.5
Triplet	Baseline	66.4	78.1	85.6
	Proposed	68.3	78.9	86.5
Quadruplet	Baseline	64.7	75.6	85.2
	Proposed	66.4	77.0	85.2

	CUB	CARS	SOP
	R-1	R-1	R-1k
Lifted [14]	47.2	49.0	97.4
N-pair [15]	51.0	71.1	97.8
P-NCA [16]	49.2	73.2	-
HDC [17]	53.6	73.7	97.7
BIER [18]	55.3	78.0	98.0
ABE [19]	58.6	82.7	98.0
MS [20]	65.7	84.1	98.7
HDML [21]	53.7	79.1	-
DeML [22]	65.4	86.3	98.1
Ours	68.3	86.3	98.8

Table 1. Left: Ablation on CUB. **Right:** Results on CUB, CARS, and SOP. All numbers in %.

we compare the performance of our method with competing, state-of-the-art metric learning methods in Table 1 (Middle), where we note our method (with the triplet variant) is quite competitive, with R-1 performance improvement of 2.6% on CUB, matching (with DeML) R-1 and slightly better R-1k performance (w.r.t. MS [20]) on SOP. We emphasize that in addition to these competitive numbers, our method is also able to provide reasoning in the form of attention maps, as discussed above, unlike these competing methods that are not able to do so.

3.2 Person re-identification

Since re-id is a special case of image retrieval, our method is certainly applicable, and we conduct experiments on CUHK03-NP detected (“CUHK”) [23,24] and DukeMTMC-reid (“Duke”) [25,26] datasets, following the protocol in Sun *et al.* [27]. We use the baseline architecture of Sun *et al.* [27], set $\gamma = 0.2$ and train the model for 40 epochs with the Adam optimizer. We show attention maps with our method in Fig. 5 where we highlight (in red) image regions that the model reasons as being important for them to represent the same person (*e.g.*, the white bag in the middle column). A key difference between our result and those in CASN [11] is that we do not need a BCE classification term to generate these attention maps. Furthermore, we do not make any re-id specific design choices (*e.g.*, upright pose assumption for attention consistency in CASN [11], hard attention in HA-CNN [28], attentive feature refinement and alignment in DuATM [29]) and are able to obtain meaningful visual explanations. We also report quantitative performance in Table 2, where we note our method achieves competitive performance: about 3% rank-1 performance improvement on CUHK and very close performance (88.5% rank-1) to the best performing method (MGN) on Duke.

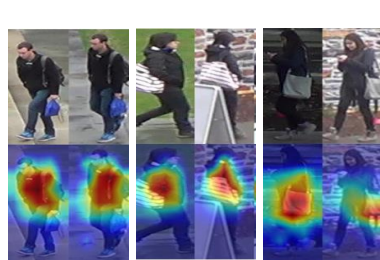


Fig. 5. Positive pair re-id attention maps.

	CUHK		Duke	
	R-1	mAP	R-1	mAP
SVD [30]	41.5	37.3	76.7	56.8
HA [28]	41.7	38.6	80.5	63.8
DA [29]	-	-	81.8	64.6
PCB [27]	63.7	57.5	83.3	69.2
MGN [31]	66.8	66.0	88.7	78.4
CASN [11]	71.5	64.4	87.7	73.7
Ours	74.5	67.5	88.5	75.8

Table 2. Re-Id results on CUHK and Duke (%)

3.3 Weakly supervised one-shot semantic segmentation

In the one-shot semantic segmentation task, we are given a test image and a pixel-level semantically labeled support image, and we are to semantically segment the test image. Given that we learn similarity predictors, we can use our model to establish correspondences between the test and the support images. One aspect that is particularly appealing with our method is explainability, and the resulting similarity attention maps we generate can be used as cues to perform semantic segmentation.

We use the PASCAL-5ⁱ dataset (“Pascal”) [32] for all experiments, following the same protocol as Shaban *et al.* [32]. Given a test image and the corresponding

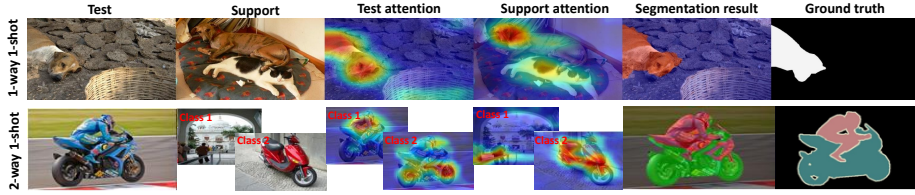


Fig. 6. Qualitative one-shot segmentation results from the PASCAL-5i dataset.

support image, we first use our trained model to generate two similarity attention maps, one for each image. We then use the attention map for the test image as a cue to generate the final segmentation mask using the GrabCut [33] algorithm. We call this the “1-way 1-shot” experiment. In the “2-way 1-shot” experiment, the test image has two objects of different classes and we are given two support images, one for each class. In this case, to generate results for object class 1, we use the support image for this object class as the positive image and the other support image as negative. Similarly, to generate results for object 2, we use the support image for this object class as the positive image and other as negative. The “2-way 5-shot” experiment is similar; the only difference is we now have five support images for each of the two classes (instead of one image as above). We first show some qualitative results in Fig. 6 (left to right: test image, support image, test attention map, support image attention map, predicted segmentation mask, ground truth mask). In the first row (1-way 1-shot), we see that, in the test attention map, our method is able to capture the “dog” region in the test image despite the presence of a “cat” in the support image, helping generate the final segmentation result. In the second row (2-way 1-shot), we see our method is able to disambiguate and segment out both the person and the bike following the person and bike categories present in the two support images.

Finally, we also report the 1-way (following the protocol of [32]) and 2-way (following the protocol of [34]) meanIOU results in Table 3. Here, despite competing methods specifically trained for the one-shot segmentation task, using a support image label mask, and being trained on relevant data (Pascal), our method gives very competitive performance. These results provide additional evidence for the generalizability of our proposed similarity attention maps (in this case they capture the similarity between the test and support images). Note that these attention maps were generated using a model trained with CUB and CARS, irrelevant data when compared to Pascal.

4 Summary and Future Work

We presented new techniques to explain and visualize, with gradient-based attention, predictions of similarity models. We showed our resulting *similarity* attention is generic and applicable to many commonly used similarity architectures. We presented a new paradigm for learning similarity functions with our *similarity mining* learning objective, resulting in improved downstream model

Methods	Mask	5 ⁰	5 ¹	5 ²	5 ³	Mean	Methods	Mask	1-shot	5-shot
OSVOS [35]	Yes	24.9	38.8	36.5	30.1	32.6	PL [34]	Yes	39.7	40.3
OSLM [32]	Yes	33.6	55.3	40.9	33.5	40.8	PL+SEG [34]	Yes	41.9	42.6
co-FCN [36]	Yes	36.7	50.6	44.9	32.4	41.1	PL+SEG+PT [34]	Yes	42.7	43.7
PAN-init [37]	Yes	30.8	40.7	38.3	31.4	35.3	Proposed	No	56.9	60.1
Proposed	No	37.9	50.3	44.4	33.8	41.6				

Table 3. Results (%) on PASCAL-5ⁱ. **Left:** 1-way 1-shot. **Right:** 2-way 1-shot and 5-shot.

performance. We also demonstrated the versatility of our framework in learning models for several diverse applications, *e.g.*, image retrieval (including re-id) and low-shot semantic segmentation. Our results also suggest that the similarity explanations can be used to address a variety of label propagation problems that need a first step of correspondence learning. With our similarity attention, we can establish such correspondences in an unsupervised fashion, opening new avenues for advances in zero- or few-shot learning. Our method could also find use in targeted retrieval for medical applications where a doctor can “tag” a certain region in the image under examination and retrieve relevant “similar” historical records for further diagnosis.

References

1. Matthew D Zeiler and Rob Fergus. Visualizing and understanding convolutional networks. In *ECCV*, 2014.
2. Aravindh Mahendran and Andrea Vedaldi. Understanding deep image representations by inverting them. In *CVPR*, 2015.
3. Bolei Zhou, Aditya Khosla, Agata Lapedriza, Aude Oliva, and Antonio Torralba. Learning deep features for discriminative localization. In *CVPR*, 2016.
4. Ramprasaath R. Selvaraju, Michael Cogswell, Abhishek Das, Ramakrishna Vedantam, Devi Parikh, and Dhruv Batra. Grad-cam: Visual explanations from deep networks via gradient-based localization. In *ICCV*, 2017.
5. Kunpeng Li, Ziyan Wu, Kuan-Chuan Peng, Jan Ernst, and Yun Fu. Tell me where to look: Guided attention inference network. In *CVPR*, 2018.
6. Lezi Wang, Ziyan Wu, Srikrishna Karanam, Kuan-Chuan Peng, Rajat Vikram Singh, Bo Liu, and Dimitris Metaxas. Sharpen focus: Learning with attention separability and consistency. In *ICCV*, 2019.
7. Dzmitry Bahdanau, Kyunghyun Cho, and Yoshua Bengio. Neural machine translation by jointly learning to align and translate. In *ICLR*, 2015.
8. Jacob Andreas, Marcus Rohrbach, Trevor Darrell, and Dan Klein. Neural module networks. In *CVPR*, pages 39–48, 2016.
9. Fei Wang, Mengqing Jiang, Chen Qian, Shuo Yang, Cheng Li, Honggang Zhang, Xiaogang Wang, and Xiaoou Tang. Residual attention network for image classification. In *CVPR*, 2017.
10. Ashish Vaswani, Noam Shazeer, Niki Parmar, Jakob Uszkoreit, Llion Jones, Aidan N. Gomez, Łukasz Kaiser, and Illia Polosukhin. Attention is all you need. In *NIPS*, 2017.
11. Meng Zheng, Srikrishna Karanam, Ziyan Wu, and Richard J Radke. Re-identification with consistent attentive siamese networks. In *CVPR*, 2019.

12. Catherine Wah, Steve Branson, Peter Welinder, Pietro Perona, and Serge Belongie. The caltech-ucsd birds-200-2011 dataset. 2011.
13. Jonathan Krause, Michael Stark, Jia Deng, and Li Fei-Fei. 3d object representations for fine-grained categorization. In *Proceedings of the IEEE International Conference on Computer Vision Workshops*, pages 554–561, 2013.
14. Hyun Oh Song, Yu Xiang, Stefanie Jegelka, and Silvio Savarese. Deep metric learning via lifted structured feature embedding. In *CVPR*, 2016.
15. Kihyuk Sohn. Improved deep metric learning with multi-class N-pair loss objective. In *NIPS*. 2016.
16. Yair Movshovitz-Attias, Alexander Toshev, Thomas K. Leung, Sergey Ioffe, and Saurabh P. Singh. No fuss distance metric learning using proxies. In *ICCV*, 2017.
17. Yuhui Yuan, Kuiyuan Yang, and Chao Zhang. Hard-aware deeply cascaded embedding. In *ICCV*, 2017.
18. Michael Opitz, Georg Waltner, Horst Possegger, and Horst Bischof. BIER - boosting independent embeddings robustly. In *ICCV*, 2017.
19. Wonsik Kim, Bhavya Goyal, Kunal Chawla, Jungmin Lee, and Keunjoo Kwon. Attention-based ensemble for deep metric learning. In *ECCV*, 2018.
20. Xun Wang, Xintong Han, Weiling Huang, Dengke Dong, and Matthew R. Scott. Multi-similarity loss with general pair weighting for deep metric learning. In *CVPR*, 2019.
21. Wenzhao Zheng, Zhaodong Chen, Jiwen Lu, and Jie Zhou. Hardness-aware deep metric learning. In *CVPR*, 2019.
22. Binghui Chen and Weihong Deng. Hybrid-attention based decoupled metric learning for zero-shot image retrieval. In *CVPR*, 2019.
23. Wei Li, Rui Zhao, Tong Xiao, and Xiaogang Wang. DeepReID: Deep filter pairing neural network for person re-identification. In *CVPR*, 2014.
24. Zhun Zhong, Liang Zheng, Donglin Cao, and Shaozi Li. Re-ranking person re-identification with k-reciprocal encoding. In *CVPR*, 2017.
25. Ergys Ristani, Francesco Solera, Roger Zou, Rita Cucchiara, and Carlo Tomasi. Performance measures and a data set for multi-target, multi-camera tracking. In *ECCVW*, 2016.
26. Zhedong Zheng, Liang Zheng, and Yi Yang. Unlabeled samples generated by gan improve the person re-identification baseline in vitro. In *ICCV*, 2017.
27. Yifan Sun, Liang Zheng, Yi Yang, Qi Tian, and Shengjin Wang. Beyond part models: Person retrieval with refined part pooling (and a strong convolutional baseline). In *ECCV*, 2018.
28. Wei Li, Xiatian Zhu, and Shaogang Gong. Harmonious attention network for person re-identification. In *CVPR*, 2018.
29. Jianlou Si, Honggang Zhang, Chun-Guang Li, Jason Kuen, Xiangfei Kong, Alex C Kot, and Gang Wang. Dual attention matching network for context-aware feature sequence based person re-identification. In *CVPR*, 2018.
30. Yifan Sun, Liang Zheng, Weijian Deng, and Shengjin Wang. SVDNet for pedestrian retrieval. In *ICCV*, 2017.
31. Guanshuo Wang, Yufeng Yuan, Xiong Chen, Jiwei Li, and Xi Zhou. Learning Discriminative Features with Multiple Granularities for Person Re-Identification. In *ACM MM*, 2018.
32. Amirreza Shaban, Shravy Bansal, Zhen Liu, Irfan Essa, and Byron Boots. One-shot learning for semantic segmentation. In *BMVC*, 2017.
33. Carsten Rother, Vladimir Kolmogorov, and Andrew Blake. Grabcut: Interactive foreground extraction using iterated graph cuts. In *ACM transactions on graphics (TOG)*, volume 23, pages 309–314, 2004.

34. Nanqing Dong and Eric P. Xing. Few-shot semantic segmentation with prototype learning. In *BMVC*, 2018.
35. Sergi Caelles, Kevins-Kokitsi Maninis, Jordi Pont-Tuset, Laura Leal-Taixé, Daniel Cremers, and Luc Van Gool. One-shot video object segmentation. In *CVPR*, 2017.
36. Kate Rakelly, Evan Shelhamer, Trevor Darrell, Alyosha Efros, and Sergey Levine. Conditional networks for few-shot semantic segmentation. In *ICLR Workshops*, 2018.
37. K. Wang, J. H. Liew, Y. Zou, D. Zhou, and J. Feng. Panet: Few-shot image semantic segmentation with prototype alignment. In *ICCV*, 2019.